Noise Analysis and Comparison of Phase- and Frequency-Detecting Readout Systems: Application to SAW Delay Line Magnetic Field Sensor

Phillip Durdaut, *Student Member, IEEE*, Anne Kittmann, Enrico Rubiola, *Member, IEEE*, Jean-Michel Friedt, Eckhard Quandt, Reinhard Knöchel, *Life Fellow, IEEE*, and Michael Höft, *Senior Member, IEEE*

***Abstract*— Transmission surface acoustic wave (SAW) sensors are widely used in various fields of application. In order to improve the limit of detection (LOD) of such sensor systems, it is essential to understand and quantify the relevant noise sources. Only then, strategies for noise reduction can be developed. In this paper, low noise readout systems for the application with SAW sensors in open-loop and closed-loop configurations are presented and experimentally investigated with regard to their phase noise on the example of a SAW delay line magnetic field sensor. Besides a comprehensive analysis of the phase- and frequency modulated signals, respectively, previously derived equations in a theoretic study for describing the LOD of both readout structures are utilized in the experimental context. According to the theory, the same LOD is also obtained in the experiment for all frequencies for which the noise contributions of the readout electronics are negligible. To the best of our knowledge, this is the first experimental study that directly compares both operating modes for the same sensor and in terms of the overall achievable LOD. The results are applicable to all kinds of phase-sensitive delay-line sensors.**

***Index Terms*— Delay line sensor, frequency detection, magnetic field detection, open-loop vs. closed-loop, phase detection, phase noise, readout systems, surface acoustic wave sensor.**

Manuscript received April 1, 2019; revised May 1, 2019; accepted May 2, 2019. Date of publication May 7, 2019; date of current version August 15, 2019. This work was supported in part by the German Research Foundation Deutsche Forschungsgemeinschaft (DFG) through the Collaborative Research Centre under Grant CRC 1261 *Magnetoelectric Sensors: From Composite Materials to Biomagnetic Diagnostics*, in part by the ANR Programme d'Investissement d'Avenir (PIA) under the Oscillator IMP Project under Grant 11-EQPX-0033, in part by the FIRST-TF Network under Grant 10-LABX-0048, and in part by the Région Bourgogne Franche-Comté intended to support the PIA. The associate editor coordinating the review of this paper and approving it for publication was Prof. Yu-Te Liao. *(Corresponding author: Phillip Durdaut.)*

P. Durdaut, R. Knöchel, and M. Höft are with the Chair of Microwave Engineering, Faculty of Engineering, Institute of Electrical Engineering and Information Technology, Kiel University, 24143 Kiel, Germany (e-mail: pd@tf.uni-kiel.de).

A. Kittmann and E. Quandt are with the Chair of Inorganic Functional Materials, Faculty of Engineering, Institute for Materials Science, Kiel University, 24143 Kiel, Germany.

E. Rubiola is with the Department of Time and Frequency, FEMTO-ST Institute, Université de Bourgogne Franche-Comté (UBFC), 25000 Besançon, France, also with the CNRS, ENSMM, 25000 Besançon, France, and also with the Physics Metrology Division, Istituto Nazionale di Ricerca Metrologica (INRiM), 10135 Turin, Italy.

J.-M. Friedt is with the Department of Time and Frequency, FEMTO-ST Institute, Université de Bourgogne Franche-Comté (UBFC), 25000 Besançon, France, and also with the CNRS, ENSMM, 25000 Besançon, France.

Digital Object Identifier 10.1109/JSEN.2019.2914965

I. Introduction

SURFACE acoustic wave (SAW) devices started to become attractive with the invention of the interdigital transducer (IDT) in 1965 [1] which allows to excite SAWs on piezoelectric substrates in an efficient way. Advantageous properties like small size, low cost, and high reproducibility [2] make SAW technology very attractive for sensor applications [3], [4]. Among many others, SAW sensors for measuring temperature [5], [6], pressure [7], [8], magnetic fields [9]–[21], humidity [22], and vibration [23] or for the detection of gases [24] and biorelevant molecules [25], [26], respectively, have been reported.

A SAW is excited by applying an electrical field on an IDT that is patterned on a piezoelectric material. The resulting mechanical wave propagates perpendicular to the direction of the IDT in both directions on the surface of the piezoelectric substrate with typical wave velocities between 3000 m/s and 5000 m/s [4], [27]. For sensing applications the substrate's surface is frequently coated with an additional layer which reacts to changes of the physical quantity to be measured, and in turn alters the SAW in its amplitude and in its velocity.

Throughout this paper, we solely focus on a two-port delay line sensor that comprises two IDT electrodes placed at some distance to each other, typically in the millimeter range. A sensing layer between the IDTs attenuates and affects the velocity of the propagating wave in dependence of the physical quantity to be measured. Because a surface acoustic wave is traveling about five orders of magnitude slower compared to the electromagnetic propagation the delay line results in typical group delays τ_g from several hundred nanoseconds to several microseconds.

There are two different schemes for the readout of SAW delay line sensors. A straightforward approach is to compare the phase of the sensor's output signal with a reference phase [27] in an open-loop system, thus creating a delay line phase discriminator [28], [29]. Alternatively, readout of such sensors can be achieved with a closed-loop approach by including the sensor into the feedback loop of an oscillator, thus changing oscillation frequency with the sensing function [30]–[32]. Both approaches might suffer from noise which is introduced into the sensor system by the required electrical components. However, even if all the electronic

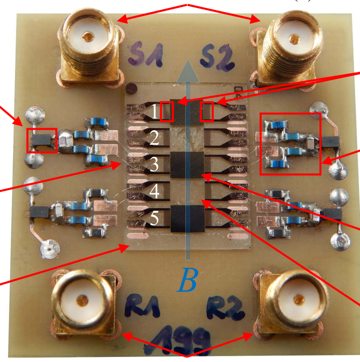

Fig. 1. Photograph of the utilized SAW delay line sensor mounted to a carrier PCB. The chip offers a total of five delay lines of which the channels 1, 3, and 5 are coated with magnetostrictive material. For this study only channels 3 (sensor) and 4 (reference) are used. The magnetic flux density B is perpendicular to the surface acoustic wave's propagation direction.

components are designed very carefully such that their noise contributions can be neglected, one crucial question remains: is one of these approaches superior to the other regarding the overall achievable limit of detection (LOD)? Recently, we addressed this question in a theoretic study [33]. In this paper, a SAW delay line magnetic field sensor is operated in open-loop configuration and in a closed-loop system. Based on phase noise measurements of the individual electronic components of both systems, the earlier presented theoretical expressions for phase noise and LOD are experimentally verified.

This paper is organized as follows: Sec. II briefly introduces the SAW magnetic field sensor utilized in this investigation. Based on the sensor-specific requirements open-loop and closed-loop readout systems are presented in Sec. III. A comparison regarding the readout system's overall phase noise is presented in Sec. IV based on the individual phase noise contributions of both the electrical components and the sensor-intrinsic noise. This article concludes with a summary in Sec. V.

II. SAW Sensor

The SAW delay line sensor has been produced in the Kiel Nano laboratory and is based on a 500 μm thick ST-cut quartz substrate. A delay line is formed using two split-finger IDT electrodes with 25 finger pairs, a periodicity of 28 μm and a finger width of 3.5 μm with an IDT center-to-center length of $L = 4.64$ mm. A SiO_2 layer with a thickness of 4.5 μm deposited on top of the IDTs and the delay line acts as a guiding layer for the surface acoustic Love wave. A magnetostrictive material $(Fe_{90}Co_{10})_{78}Si_{12}B_{10}$ with a thickness of 200 nm and a length of 3.8 mm is deposited on top of the guiding layer and between the IDTs. Further details about the fabrication can be found in [19].

Fig. 1 shows a photograph of the SAW delay line sensor. The quartz-based chip offers a total of five delay lines of which the channels 1, 3, and 5 are coated with magnetostrictive material. For this study only channels 3 (sensor) and the magnetically uncoated channel 4 (reference) are used. The chip is mounted to a printed circuit board (PCB) which mainly contains discrete inductors and capacitors for the matching of the electrical impedance of both channels to 50 Ω. In order to suppress significant signal-dropping in the transmission characteristics due to interference of electrical crosstalk, the delay lines are connected symmetrically utilizing baluns (*ATB2012E-50011* from *TDK*) at each port.

The sensor principle [19] is based on the magnetoelastic effect which changes the shear modulus of the magnetostrictive material as a function of the material's magnetization, i.e. by a surrounding magnetic flux density B. Due to the relation between the elastic properties and the wave's propagation velocity [10], the phase angle φ of the sensor signal changes with the magnetic flux density B.

For this type of sensor, not only the expected dependence of the magnetic sensitivity $\mathcal{S}_{\mathrm{mag}}$ on a DC magnetic bias flux density B_{bias} exists, but also strong interdependencies between the magnetic insertion loss $\mathrm{IL}_{\mathrm{mag}}$, the sensor's intrinsic phase noise and both the SAW input power P_{SAW} and B_{bias} are observed. There is evidence that such behavior can be explained by the nonlinear characteristic of the magnetostrictive material and by power-dependent hysteresis losses. Generally, an additional DC bias flux density B_{bias} can be applied to minimize the phase noise and thus, improve the limit of detection (LOD). However, this requires the sensor to be surrounded by an additional coil fed by a current from an ultra-low noise current source which is also capable of providing relatively high currents in order to perform a certain magnetic saturation prior to the measurements. Yet, the sensor used in this investigation is quite suited to operate without any DC bias flux density. For simplification, and because the focus in this article is on the readout systems, the magnetic operating point is set to $B_{\mathrm{bias}} = 0$. Tab. I summarizes the most important electrical and magnetic properties of the SAW magnetic field sensor in its operating point. Compared to the magnetic sensitivity reported in [19], the value of $\mathcal{S}_{\mathrm{mag}}$ increased roughly by a factor two to three (depending on B_{bias}) which results from an improved control of the parameters during deposition of the magnetostrictive layer. This leads to a more defined magnetic anisotropy and with that to a higher sensitivity.

III. Readout Systems

The developed open- and closed-loop readout systems are depicted in Fig. 2 together with the according power levels. Both systems are mostly based on RF components by *Mini-Circuits* with all their identifiers given in the system diagrams. In order to allow a comparison between both methods, care has been taken to feed the SAW sensor in each case with the same input power of $P_{\mathrm{SAW}} = 0$ dBm because the SAW sensor's intrinsic phase noise of this special kind of magnetically coated delay line sensor is a function of P_{SAW} (see Sec. II).

A. Open-Loop System

The open-loop readout system (Fig. 2a) [19] is based on a heterodyne structure in which the output signal of a phase stable numerically controlled oscillator (NCO) with a frequency of 50 kHz is upconverted to the SAW device's passband at $f_0 = 144.8$ MHz by means of a single sideband (SSB) upconverter and a local oscillator (LO). The SSB upconverter

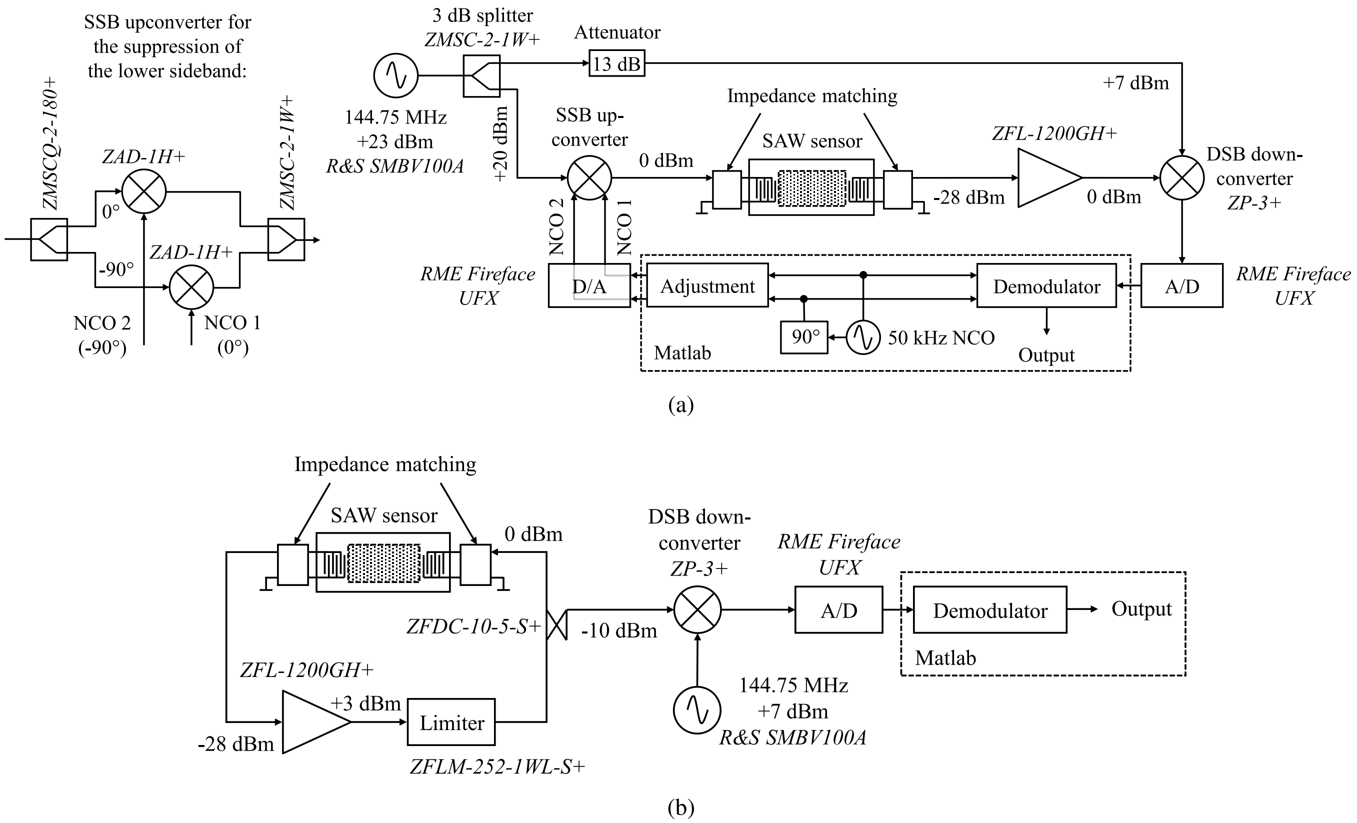

Fig. 2. Developed open- and closed-loop readout systems for the determination of the applied magnetic field. In the open-loop systems a magnetic flux density to be measured leads to a phase modulation of the SAW sensor's output signal whereas the same leads to a frequency modulation in the closed-loop oscillator. (a) Open-loop readout system with inherent phase noise suppression of the high-frequency local oscillator. A low phase noise signal of a numerically controlled oscillator (NCO) with a frequency of 50 kHz is transposed to the SAW sensor's operating frequency $f_0 = 144.8$ MHz and received using a floating local oscillator, which largely suppresses its phase noise. Phase detection is performed in the digital domain after analog-to-digital (A/D) conversion. The insert on the left depicts the internal structure of the single sideband (SSB) upconverter. (b) Closed-loop readout system with the SAW sensor included in the feedback loop of an amplifier leading to an oscillation with a frequency of approx. $f_0 = 144.8$ MHz. A limiter is used to stabilize the SAW sensor's input power to 0 dBm. Frequency detection is performed in the digital domain after downconverting the oscillation signal to an intermediate frequency of 50 kHz and subsequent analog-to-digital (A/D) conversion.

suppresses the undesired lower sideband which would also fall into the passband of the SAW device and which represents the image frequency with regard to the subsequent downconverter. Sufficient sideband suppression (typically about -60 dB) is achieved by adjusting both amplitude and phase of the SSB converter drive signals numerically. The SSB upconverter consists of a 2-way-90° power splitter *ZMSCQ*-2-180+ at the input and a 2-way-0° combiner *ZMSC*-2-1*W*+ at the output. In-between, two level-17 mixers *ZAD*-1*H*+ perform the frequency conversion (see Fig. 2a). The sensor's output signal is amplified and downconverted to the original frequency of 50 kHz utilizing a double sideband (DSB) mixer using the same LO. Thus, the phase noise of the high-frequency LO is largely suppressed. In fact, the degree of phase noise suppression depends on the group delay τ_g of the SAW sensor and on the offset frequency [34]. Final phase detection is performed in the digital domain, i.e. with Matlab, using quadrature signal processing after analog-to-digital (A/D) conversion utilizing an A/D converter *RME Fireface UFX* with a sample rate of 192 kHz. In a frequency span of ± 1 kHz around the intermediate frequency of 50 kHz the converter offers a spurious-free dynamic range (SFDR) of 123.5 dB yielding an effective number of bits (ENOB) of 16.2 bit. However, the quantization noise floor is even 138.4 dB below the carrier amplitude. Thus, in a bandwidth of 1 Hz the ENOB is even 22.7 bit when neglecting the spurious signals. Assuming a sinusoidal magnetic flux density to be measured $B_x(t) = \hat{B}_x \cos(2\pi f_x t)$ the sensor's output signal

$$s_{PM}(t) \propto \cos\left(2\pi f_0\ t + \mathcal{S}_{PM} \hat{B}_x \cos(2\pi f_x t) + \psi_{OL}(t)\right) \quad (1)$$

is phase modulated (PM) by $B_x(t)$ with a sensitivity of $\mathcal{S}_{PM} = \mathcal{S}_{mag} = 16.5$ rad/mT ($\approx$ 945°/mT). Note that Eq. (1) is true for any kind of phase-sensitive sensor, e.g. for a temperature sensor for which $B_x(t)$ would represent the unknown temperature while the sensitivity $\mathcal{S}_{PM}$ would then have the physical dimension rad/K. From basic modulation theory, it is well-known that the modulation index $\eta_{PM} = \mathcal{S}_{PM} \hat{B}_x$ is linked to the carrier-to-sideband ratios of phase-modulated signals by *Bessel functions* of the first kind $J_\nu(\eta_{PM})$, where ν is the number of the sideband (SB) [35, p. 141 ff.]. Based on this relationship, prior to the noise measurements, the modulation purity and thus, the sensitivity $\mathcal{S}_{PM}$ is verified by a series of measurements for various amplitudes $\hat{B}_x$ of the signal to be measured with the results shown in Fig. 3a. In Eq. (1) $\psi_{OL}(t)$ describes the overall phase noise of the open-loop system, i.e. the phase noise of the SAW sensor and the phase noise of the electronic readout system. Both, the contribution of the sensor

TABLE I
SUMMARY OF THE ELECTRICAL AND MAGNETIC PROPERTIES OF THE UTILIZED MAGNETIC FIELD SAW SENSOR IN ITS OPERATING POINT

Length of the delay line	$L = 4.64\,\mathrm{mm}$
Acoustic wavelength	$\lambda = 28\,\mu\mathrm{m}$
Center frequency	$f_0 = 144.8\,\mathrm{MHz}$
$-3\,\mathrm{dB}$ bandwidth	$\Delta f = 4.6\,\mathrm{MHz}$
Return loss	$\mathrm{RL} > 20\,\mathrm{dB}$
Insertion loss of the delay line	$\mathrm{IL}_{\mathrm{elec}} = 20\,\mathrm{dB}$
Magnetic loss	$\mathrm{IL}_{\mathrm{mag}} = 8\,\mathrm{dB}$
Overall insertion loss	$\mathrm{IL} = \mathrm{IL}_{\mathrm{elec}} + \mathrm{IL}_{\mathrm{mag}} = 28\,\mathrm{dB}$
Phase velocity	$v_\varphi = f_0\lambda = 4054\,\mathrm{m/s}$
Phase delay	$\tau_\varphi = L/v_\varphi = 1145\,\mathrm{ns}$
Phase slope of the delay line	$\partial\varphi/\partial f = -8.73\,\mathrm{rad/MHz}$
Group delay	$\tau_{\mathrm{g}} = -\partial\varphi/(\partial f\ 2\pi) = 1389\,\mathrm{ns}$
Group velocity	$v_{\mathrm{g}} = L/\tau_{\mathrm{g}} = 3341\,\mathrm{m/s}$
Electrical sensitivity	$\mathcal{S}_{\mathrm{elec}} = 2\pi\tau_{\mathrm{g}} = 8.73\,\mathrm{rad/MHz}$
Magnetic sensitivity	$\mathcal{S}_{\mathrm{mag}} = \partial\varphi/\partial B = 16.5\,\mathrm{rad/mT}$
SAW input power	$P_{\mathrm{SAW}} = 0\,\mathrm{dBm}$
Magnetic operating point	$B_{\mathrm{bias}} = 0$
Sensor's phase noise $S_\varphi(f)$	See Fig. 4

as well as the individual contributions of the various electrical components will be analyzed in Sec. IV.

B. Closed-Loop System

The structure of the closed-loop readout system is shown in Fig. 2b. The SAW sensor is included in the feedback branch of an amplifier which compensates for the sensor's insertion loss, and thus leads to an oscillation at approx. $f_0 = 144.8$ MHz. An additional limiter is used to stabilize the SAW sensor's input power to 0 dBm. Because of the sensor's linear phase response over a wide frequency range with a slope of $\partial\varphi/\partial f = -8.73$ rad/MHz, oscillations with a frequency spacing of $\delta f_0 = 1/\tau_{\mathrm{g}} \approx 720$ kHz $< \Delta f$ are generally possible. Therefore, an additional phase shifter is not needed. Utilizing a -10 dB directional coupler the oscillator signal is coupled into a mixer for downconversion to an intermediate frequency of 50 kHz in order to perform the subsequent analog-to-digital conversion and the demodulation. The frequency demodulation is also carried out in Matlab and the analog-to-digital (A/D) conversion is performed with the same A/D converter as in the open-loop system. Assuming again a sinusoidal magnetic flux density to be measured $B_{\mathrm{x}}(t) = \hat{B}_{\mathrm{x}} \cos(2\pi f_{\mathrm{x}} t)$ the oscillator signal

$$s_{\mathrm{FM}}(t) \propto \cos\left(2\pi f_0\ t + \frac{\mathcal{S}_{\mathrm{FM}}\hat{B}_{\mathrm{x}}}{f_{\mathrm{x}}} \sin(2\pi f_{\mathrm{x}} t) + \psi_{\mathrm{CL}}(t)\right) \quad (2)$$

is frequency modulated (FM) by $B_{\mathrm{x}}(t)$ with a sensitivity of $\mathcal{S}_{\mathrm{FM}} = \mathcal{S}_{\mathrm{mag}}/\mathcal{S}_{\mathrm{elec}} = 1.9$ MHz/mT or with a modulation index of $\eta_{\mathrm{FM}} = \mathcal{S}_{\mathrm{FM}}\hat{B}_{\mathrm{x}}/f_{\mathrm{x}}$, respectively. Again, note that Eq. (2) is also true for any kind of phase-sensitive sensor, e.g. for a temperature sensor for which $B_{\mathrm{x}}(t)$ would represent the unknown temperature while the sensitivity $\mathcal{S}_{\mathrm{FM}}$ would then have the physical dimension Hz/K. As already shown for the open-loop system, the FM purity and the sensitivity $\mathcal{S}_{\mathrm{FM}}$ is verified by measurements of the carrier-to-sideband ratios and subsequent comparison with the theoretical expectations

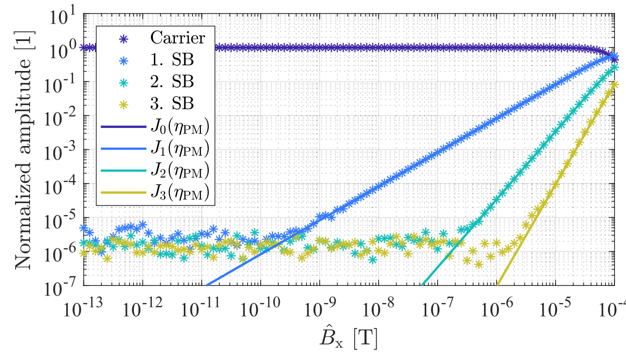

(a)

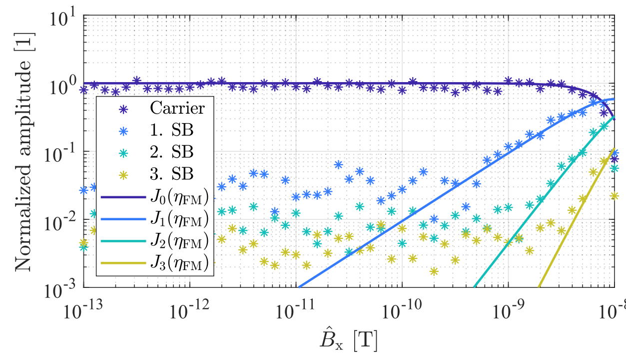

(b)

Fig. 3. Verification of the modulation purities for both sensor systems (Fig. 2) by measured carrier and sideband (SB) amplitudes (markers) of the modulated signals after analog-to-digital conversion and comparison with the theoretical expectations (solid lines). The measurements were conducted for a frequency $f_{\mathrm{x}} = 10$ Hz with the sensor in its operating point according to Tab. I. (a) Phase modulated signal in the open-loop system. (b) Frequency modulated signal in the closed-loop system.

according to the *Bessel functions* of the first kind $J_\nu(\eta_{\mathrm{FM}})$. The results are shown in Fig. 3b in which the variance of the measured amplitudes is distinctly higher as for the PM case because of the high phase noise in the closed-loop-system. In Eq. (2) $\psi_{\mathrm{CL}}(t)$ describes the overall oscillator phase noise of the closed-loop system, i.e. the phase noise due to the SAW sensor and due to the electronic readout system, both further discussed in Sec. IV.

IV. NOISE ANALYSIS

Random fluctuations of an arbitrary phase $\varphi(t)$ are best described by the one-sided power spectral density of the random phase fluctuations $S_\varphi(f)$ in units of rad^2/Hz. For historical reasons, phase noise analyzers give the results in terms of a phase noise density spectrum $\mathscr{L}(f)$ which is defined as $\mathscr{L}(f) = 1/2\ S_\varphi(f)$ and usually given in units of dBc/Hz [36]. In order to simplify mathematical expressions and to stay with SI units, $S_\varphi(f)$ is used throughout this article. The logarithmic representation $10\log_{10}(S_\varphi(f))$ is then given in units of dB rad^2/Hz. A useful model for describing the frequency dependence of a power spectral density of random phase fluctuations is the polynomial law

$$S_\varphi(f) = \sum_{i=-n}^{0} b_i f^i \quad (3)$$

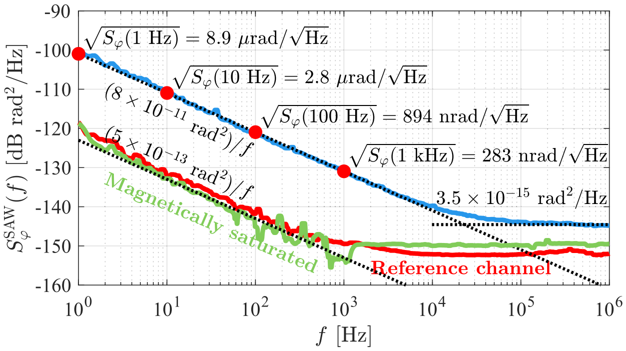

Fig. 4. Measured power spectral density of the random phase fluctuations of the SAW sensor in its operating point according to Tab. I (blue) and under magnetic saturation (green). A measurement for the magnetically uncoated reference channel (red) reveals virtually the same flicker phase noise as for the coated sensor channel under magnetic saturation (green).

with usually $n \leq 4$. $i = 0$ and $i = -1$ refer to white phase noise and $1/f$ flicker phase noise, respectively, which are the main processes in two-port components [37, p. 23] [38]. As will be shown further below, in closed-loop systems white phase noise results in white frequency noise ($i = -2$) and flicker phase noise results in flicker frequency noise ($i = -3$). Higher order effects like random walk of frequency ($i = -4$) are related to environmental changes like e.g. temperature drifts, humidity, and vibrations [39]. All phase noise measurements were performed utilizing a *Rohde & Schwarz FSWP* phase noise analyzer.

A. SAW Sensor

For the measurement of the power spectral density of the random phase fluctuations of the magnetically coated SAW device $S_\varphi^{\text{SAW}}(f)$, the sensor has been placed inside an ultra high magnetic field shielding mu-metal cylinder *ZG1* from *Aaronia AG* in order to avoid environmental magnetic distortions. For the sensor in its operating point (blue line in Fig. 4) of $B_{\text{bias}} = 0$ the measurement reveals a $1/f$ flicker phase noise which can be quantified properly by b_{-1}/f with $b_{-1} = 8 \times 10^{-11}$ rad^2. If the sensor is magnetically saturated utilizing a strong permanent magnet (green line in Fig. 4) the flicker phase noise decreases by more than 20 dB and reaches virtually the same value of $b_{-1} = 5 \times 10^{-13}$ rad^2 as for a measurement of the uncoated reference channel (red line in Fig. 4). This indicates that the sensor's resolution is limited by magnetic noise, e.g. magnetic domain wall motions, which is typical for magnetic field sensors based on magnetic thin films [40]. Although both measurements were conducted for an input power of $P_{\text{SAW}} = 0$ dBm the white phase noise level differs because under magnetic saturation the insertion loss decreases. Note that both white phase noise floors are slightly impaired by an utilized preamplifier (*ZFL*-1000LN+ from *Mini-Circuits* with a noise figure of $F \approx 3$ dB) at the RF input of the phase noise analyzer.

B. Open-Loop System

For the open-loop system, Fig. 5a depicts the measured phase noise contributions of the various electrical components. The high phase noise of the LO with values of -31 dB rad^2/Hz at 1 Hz and -74 dB rad^2/Hz at 10 Hz (not shown for clarity) is largely suppressed in the downconverter stage. The degree of phase noise suppression as a function of the frequency and the sensor's group delay

$$\text{PNS}(f, \tau_g) = 20 \log_{10}\left(2 \sin\left(\pi f \tau_g\right)\right) \text{dB} \tag{4}$$

has already been determined and was experimentally verified in previous investigations [33], [34]. Thus, the SAW sensor dominates the overall phase noise for frequencies < 1 kHz. At $f = 1$ Hz the mixers and the amplifier contribute a phase noise density of approx. -120 dB rad^2/Hz. With values < -135 dB rad^2/Hz, the phase noise of the NCOs, i.e. the in-phase and quadrature (IQ) signals are negligible at low frequencies. However, for frequencies > 1 kHz the sum of the phase noise contributions of the various electrical components become dominant and result in a white phase noise level of 7.5×10^{-14} rad^2/Hz.

The LOD of the open-loop magnetic field sensor system in units of T/$\sqrt{\text{Hz}}$ can be calculated [33] by

$$\text{LOD}_{\text{PM}}(f) = \frac{\sqrt{S_\psi^{\text{OL}}(f)}}{\mathcal{S}_{\text{PM}}}, \tag{5}$$

where $S_\psi^{\text{OL}}(f)$ is the power spectral density of the fluctuating phase $\psi_{\text{OL}}(t)$ introduced in Eq. (1). This power spectral density is the sum of both, the phase noise of the SAW sensor and the phase noise contributions of all other electrical components of the open-loop system (mixers, amplifier, NCOs, and LO with PNS) shown in Fig. 5a. Please note that Eq. (4) and Eq. (5) are simplified expressions for delay line sensors offering bandwidths higher than the frequency to be analyzed, which is true for the sensors under investigation. More accurate expressions for narrow band delay line sensors can be found in [33].

C. Closed-Loop System

For the noise analysis of the closed-loop system only the contributions of the electrical components inside the oscillator loop are relevant. In fact, these are only the phase noise of the SAW sensor and the amplifier. The phase noise spectra of the limiter and of the directional coupler are actually not measurable with the *Rohde & Schwarz FSWP* phase noise analyzer in a reasonable time because values as low as approx. -180 dB rad^2/Hz at 10 Hz can be typically found for such passive devices [41]. In addition to the intrinsic noise of the SAW sensor, Fig. 5b shows the measured phase noise of the amplifier and an estimation of the contributions of the passive components utilized inside the oscillator loop. Both the noise contributions of the passive components and the amplifier are negligible for $f < 8$ kHz. Actually, the influence of the amplifier above this frequency could easily be further decreased by utilizing a fixed-gain amplifier instead of a variable-gain amplifier used here. In order to calculate the LOD for the closed-loop sensor system it is necessary to convert the phase noise of the individual components into oscillator phase noise at the output of the oscillator, i.e. at the output of the directional coupler. Following the derivations in [33], random phase fluctuations $\varphi(t)$ fed into an ideal delay

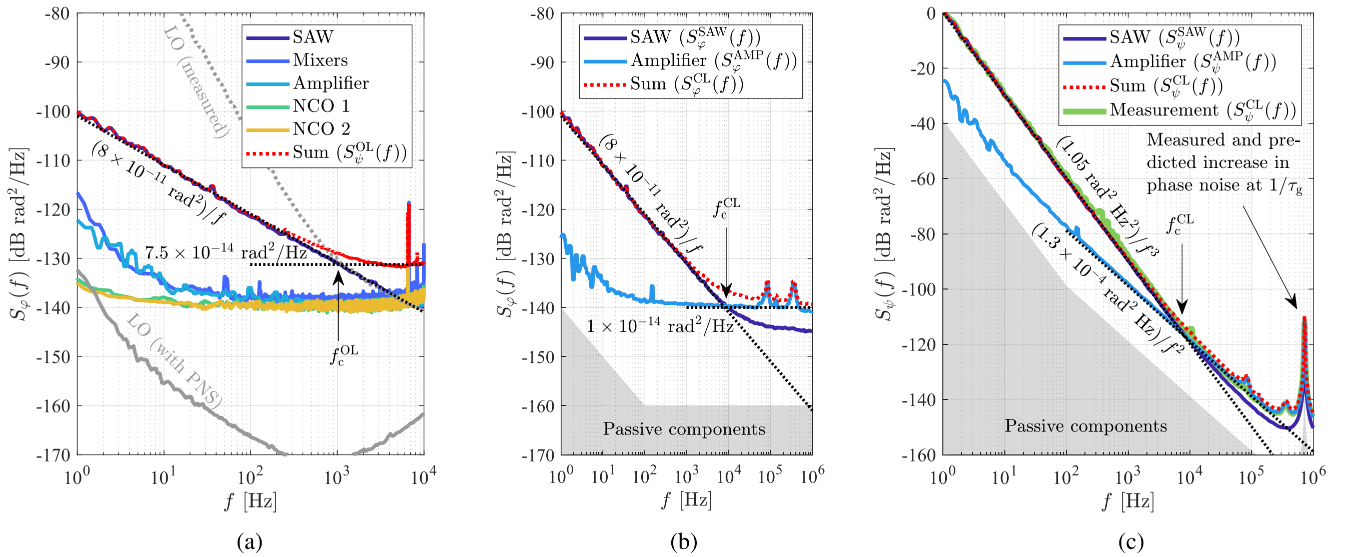

Fig. 5. Power spectral densities of the random phase fluctuations of the individual components of the open-loop sensor system (a) and of the closed-loop sensor system (b). The calculated contribution of the individual components of the closed-loop SAW sensor system to the oscillator's phase noise is in perfect agreement with a measurement of the oscillator's phase noise (c). All measurements of the individual components are performed in their operating points regarding input power, gain, and frequency exactly like depicted in Fig. 2. The arrows mark the crossover frequencies f_c^OL and f_c^CL for which the flicker phase noise is equal to the white phase noise ((a) and (b)) and for which the flicker frequency noise equals the white frequency noise (c). (a) Measured phase noise of the individual components of the open-loop SAW sensor system together with their sum. (b) Measured phase noise of the individual components of the closedloop SAW sensor system. (c) Calculated contribution to the oscillator's phase noise of the individual components of the closedloop SAW sensor system together with their sum in comparison to a measurement of the oscillator's phase noise.

line oscillator result in oscillator phase noise $\psi(t)$ according to the transfer function

$$|H(f)|^2 = \left|\frac{\Psi(f)}{\Phi(f)}\right|^2 = \frac{1}{\left|1-e^{-j2\pi f\tau_\mathrm{g}}\right|^2} = \frac{1}{2\,(1-\cos(2\pi f\tau_\mathrm{g}))} = \frac{1}{4\sin^2(\pi f\tau_\mathrm{g})}, \tag{6}$$

where $\Phi(f)$ and $\Psi(f)$ represent the Fourier transforms of the fluctuating phases $\varphi(t)$ and $\psi(t)$. A more general representation of this transfer function which also takes into account the frequency-selective characteristic of narrow band delay line sensors is given in [33]. However, the SAW sensor under investigation offers a relatively high -3 dB bandwidth of $\Delta f = 4.6$ MHz, such that the approximation in Eq. (6) is valid for the frequency range of up to 1 MHz analyzed in the following (Fig. 5 and Fig. 6). The power spectral density of the SAW delay line oscillator's overall random phase fluctuations is then given by

$$S_\psi^{\mathrm{CL}}(f) = |H(f)|^2\ S_\varphi^{\mathrm{CL}}(f). \tag{7}$$

The sum of the phase noise contributions of the SAW sensor, the amplifier, and the (negligible) passive components $S_\varphi^{\mathrm{CL}}(f) = S_\varphi^{\mathrm{SAW}}(f)+S_\varphi^{\mathrm{AMP}}(f)$ shown in Fig. 5b are converted into oscillator phase noise $S_\psi^{\mathrm{CL}}(f) = S_\psi^{\mathrm{SAW}}(f) + S_\psi^{\mathrm{AMP}}(f)$ using Eq. (7) and are shown in Fig. 5c. As one would expect, the SAW sensor is still contributing the dominant noise for $f < 8$ kHz whereas the overall noise floor is limited by the amplifier's noise for $f > 8$ kHz. The sum of the individual contributions (dotted line) perfectly agrees with a direct measurement of the oscillator's phase noise, and thus confirms the transfer function $|H(f)|^2$ from Eq. (6). Even the predicted increase in oscillator phase noise at $f = 1/\tau_\mathrm{g} \approx 720$ kHz, due to the pole of the transfer function, perfectly matches

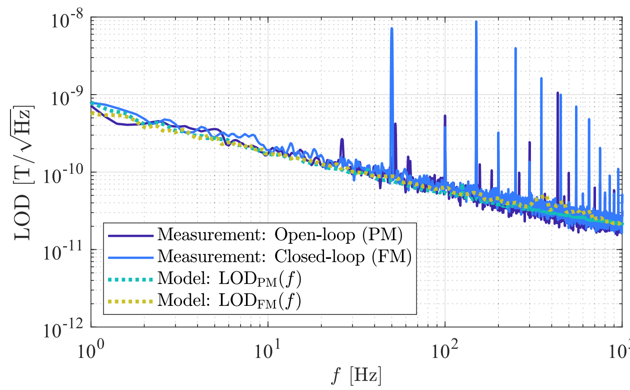

Fig. 6. Measured limits of detection (LOD) utilizing the open-loop and closed-loop readout systems presented in Sec. III compared to their predictions according to Eq. (5) and (8). Both operational modes result in the same LOD. Spurious signals are due to the power supply of the amplifiers and can be disregarded.

the measurement. With the relation between the power spectral density of arbitrary random phase fluctuations $S_\varphi(f)$ and the power spectral density of frequency fluctuations $S_{\Delta f_0}(f) = f^2\ S_\varphi(f)$ [39] in units of Hz^2/Hz and for a carrier signal of frequency f_0, the LOD of the closed-loop magnetic field sensor system in units of T/$\sqrt{\mathrm{Hz}}$ can be calculated [33] by

$$\mathrm{LOD_{FM}}(f) = \frac{\sqrt{S_{\Delta f_0}^{\mathrm{CL}}(f)}}{S_{\mathrm{FM}}} = \frac{\sqrt{f^2\ S_\psi^{\mathrm{CL}}(f)}}{S_{\mathrm{FM}}} = \frac{f\ |H(f)|\ \sqrt{S_\varphi^{\mathrm{CL}}(f)}}{S_{\mathrm{FM}}}. \tag{8}$$

D. Comparison of the Limit of Detection (LOD)

Both expressions for the LOD in the open-loop and for the closed-loop sensor system (Eq. (5) and (8)) directly scale with the amplitude spectral densities of the randomly fluctuating phase of the SAW sensor and the readout electronics. Thus, depending on how carefully the readout systems are designed in terms of phase noise, the LOD can differ. However, as shown for both systems the SAW sensor contributes the dominant phase noise at least for frequencies < 1 kHz. Thus, when assuming that the SAW sensor contributes the dominant phase noise in each system, equality between $\mathrm{LOD_{FM}}(f)$ and $\mathrm{LOD_{PM}}(f)$ can easily be shown. With Eq. (6) and for frequencies $f \ll \Delta f$ Eq. (8) can be written as

$$\mathrm{LOD_{FM}}(f) \approx \frac{f\,\sqrt{S_\varphi^{\mathrm{SAW}}(f)}}{2\sin(\pi f \tau_\mathrm{g})\;\mathcal{S}_\mathrm{FM}}. \tag{9}$$

Replacing both the sine with a small-angle approximation ($\sin(x) \approx x$) which is valid for $f\tau \ll 0.1$ and replacing $\mathcal{S}_\mathrm{FM}$ with the previously defined closed-loop sensitivity $\mathcal{S}_\mathrm{FM} = \mathcal{S}_\mathrm{mag}/\mathcal{S}_\mathrm{elec} = \mathcal{S}_\mathrm{mag}/(2\pi\tau_\mathrm{g})$, Eq. (9) yields

$$\mathrm{LOD_{FM}}(f) \approx \frac{2\pi f \tau_\mathrm{g}\,\sqrt{S_\varphi^{\mathrm{SAW}}(f)}}{2\pi f \tau_\mathrm{g}\;\mathcal{S}_\mathrm{mag}}. \tag{10}$$

With the definition of the open-loop sensitivity $\mathcal{S}_\mathrm{PM} = \mathcal{S}_\mathrm{mag}$, Eq. (10) then virtually equals the LOD of the open-loop system

$$\mathrm{LOD_{FM}}(f) \approx \frac{\sqrt{S_\varphi^{\mathrm{SAW}}(f)}}{\mathcal{S}_\mathrm{mag}} = \mathrm{LOD_{PM}}(f). \tag{11}$$

For both sensor systems presented in Sec. III the LOD was measured as described in [19] and compared with calculations based on Eq. (5) and (8). The results are shown in Fig. 6 and reveal that the measured LODs not only agree with their according predictions but also that the results are the same for open-loop (PM) and closed-loop (FM) operation for frequencies < 1 kHz. A value of approx. 170 pT/$\sqrt{\mathrm{Hz}}$ is reached at a frequency of 10 Hz.

E. Time Domain Uncertainty

The output of a sensor system is most often exploited as a stream of data averaged over a certain time interval. For the presented readout systems the output signal is provided by the phase demodulator of the open-loop system and by the frequency demodulator of the closed-loop, respectively (Fig. 2). Without any further signal processing, the time interval between two consecutive data points in both of these output signals is equal to $1/f_\mathrm{s}$, where $f_\mathrm{s} = 192$ kHz is the sample rate of the A/D converter. Thus, the data is already averaged over a time interval of $1/f_\mathrm{s} \approx 5.21\ \mu s$ due to the A/D converter's internal sample and hold circuit. According to the sampling theorem, the bandwidth is therefore limited to the theoretical value $f_\mathrm{s}/2$. For the special case of the presented open-loop system, the bandwidth is lower because the intermediate frequency of the heterodyne system has been set to 50 kHz. However, in good approximation it can be assumed that the bandwidth of both systems is several tens of kilohertz.

Depending on the application, it is generally wise to further lowpass filter the output signal. Such a filter reduces bandwidth, and in turn the white-noise power. This results in an improved time domain uncertainty, at the cost of a slower data rate. That done, it makes sense to undersample (decimate) the output data stream at the new, lower, sample rate that matches the reduced bandwidth. The undersampling process defines an averaging time τ (please do not confuse τ with the phase delay τ_φ or the group delay τ_g). In fact, the lowpass filter results from a convolution, which is a weighted sliding average, the weight function being the time-reversed impulse response.

The white noise can be reduced arbitrarily, limited only by the slowest data rate (the lowest bandwidth) that can be accepted. However, a real sensor system usually contains white noise and $1/f$ flicker noise (Fig. 5). For such a system, the question about the optimum averaging time τ_opt, beyond which the uncertainty no longer improves, arises. This question is best answered describing the fluctuations in terms of the *Allan variance* (AVAR) [42], [43]. The AVAR of an arbitrary quantity $y(t)$, denoted by $\sigma_y^2(\tau)$, is an extension of the regular variance that makes the averaging time τ appear explicitly, and also converges in the presence of flicker noise, random walk and drift. Describing random fluctuations of $y(t)$ by the power spectral density $S_y(f) = h_{-1}/f + h_0$, it holds that $\sigma_y^2(\tau) = 2\ln(2)h_{-1} + h_0/(2\tau)$. We have shown in [33] that the optimum averaging time is

$$\tau_\mathrm{opt} = \frac{1}{4\ln(2)}\frac{1}{f_\mathrm{c}} \approx 0.36\frac{1}{f_\mathrm{c}} \tag{12}$$

where $f_\mathrm{c} = h_{-1}/h_0$ is the corner frequency where the flicker noise crosses the white noise.

For the open-loop system, we identify the quantity $y(t)$ with the random phase $\varphi(t)$, thus $h_i = b_i$. With a flicker phase noise of $b_{-1} = 8 \times 10^{-11}$ rad^2 and white phase noise of $b_0 = 7.5 \times 10^{-14}$ rad^2/Hz (Fig. 5a) the corner frequency yields

$$f_\mathrm{c}^\mathrm{OL} = \frac{h_{-1}}{h_0} = \frac{b_{-1}}{b_0} = 1.07\ \text{kHz}. \tag{13}$$

For the closed-loop system, we identify the quantity $y(t)$ with the fractional frequency fluctuation $(\Delta f_0)(t)/f_0$, thus $h_{-1} = b_{-3}/f_0^2$ and $h_0 = b_{-2}/f_0^2$. With a flicker frequency noise of $b_{-3} = 1.05$ rad^2 Hz^2 and white frequency noise of $b_{-2} = 1.3 \times 10^{-4}$ rad^2 Hz (Fig. 5c) the corner frequency yields

$$f_\mathrm{c}^\mathrm{CL} = \frac{h_{-1}}{h_0} = \frac{b_{-3}}{b_{-2}} = 8.08\ \text{kHz}. \tag{14}$$

Thus, for the presented readout systems, the optimum averaging times differ and result in $\tau_\mathrm{opt}^\mathrm{OL} \approx 338\ \mu s$ and $\tau_\mathrm{opt}^\mathrm{CL} \approx 45\ \mu s$. The reason for this difference is the white noise level due to dominant noise contributions of various electrical components in the open-loop system for $f > f_\mathrm{c}^\mathrm{OL}$ (Fig. 5a). Compared to this, the amplifier of the closed-loop system has a dominant influence on the overall noise floor only for $f > f_\mathrm{c}^\mathrm{CL}$ (Fig. 5b). The equivalent magnetic uncertainties then yield $\sigma_y^\mathrm{OL}(\tau_\mathrm{opt}^\mathrm{OL})/\mathcal{S}_\mathrm{PM} \approx 903$ pT for the open-loop system and $\sigma_y^\mathrm{CL}(\tau_\mathrm{opt}^\mathrm{CL})\,f_0/\mathcal{S}_\mathrm{FM} \approx 904$ pT for the closed-loop system. These are virtually identical, because the white noise is negligible compared to the high flicker noise in this broadband view. For ideal sensor systems, in which the sensor contributes the dominant phase noise for all frequencies, or in which the system's bandwidth would be limited by a lowpass filter with a cutoff frequency $f < f_c$, τ_{opt} would be the same for both readout systems [33].

V. Conclusion

In this paper, two low noise readout systems for the application with SAW sensors are presented and compared with regard to the overall achievable LOD. The first system is designed for the differential measurement of phase changes in an open-loop configuration whereas the second system is based on a frequently used self-oscillating closed-loop structure in which a change of the sensor's phase response alters the oscillating frequency. By analyzing the phase noise contributions of the individual electrical components of each readout system it is revealed that the utilized SAW delay line magnetic field sensor contributes the dominant phase noise for a wide range of frequencies. In particular, it is shown that the phase noise of the SAW delay line oscillator, i.e. the closed-loop system, can be accurately predicted such that according expressions for the calculation of the limits of detection can be derived. Based on these equations equality between the LOD of open-loop and closed-loop SAW delay line readout can be shown even analytically assuming that the sensor contributes the dominant phase noise. This equality is verified by according measurements. These results are applicable to all kinds of phase sensitive delay line sensors. Therefore, the decision-making process for selecting a certain readout structure for a given sensor should mainly be based on the possibility to reduce the electronic's phase noise contribution. However, only open-loop systems allow for the characterization of the sensor's transmission properties as well as to identify the optimum operating point. In addition to the LOD, which was considered the most important property here, other features such as e.g. bandwidth, dynamic range, linearity, system size, immunity against environmental influences, the availability and costs of low noise electronic components, power consumption, and possibly computing power can be important in practical implementation. These properties highly depend on the application of the sensor system and are far from the focus of this article.

Acknowledgment

The authors would like to thank Wolfgang Taute for fruitful discussions and practical help during the development of the readout electronics.

References

[1] R. M. White and F. W. Voltmer, "Direct piezoelectric coupling to surface elastic waves," *Appl. Phys. Lett.*, vol. 7, no. 12, pp. 314–316, 1965.
[2] C. C. W. Ruppel *et al.*, "SAW devices for consumer communication applications," *IEEE Trans. Ultrason., Ferroelectr., Freq. Control*, vol. 40, no. 5, pp. 438–452, Sep. 1993.
[3] R. M. White, "Surface acoustic wave sensors," in *Proc. IEEE Ultrason. Symp.*, San Francisco, CA, USA, Oct. 1985, pp. 490–494.
[4] L. Bo *et al.*, "Surface acoustic wave devices for sensor applications," *J. Semicond.*, vol. 37, no. 2, pp. 021001-1–021001-9, 2016.
[5] J. Neumeister, R. Thum, and E. Lüder, "A SAW delay-line oscillator as a high-resolution temperature sensor," *Sens. Actuators A, Phys.*, vol. 22, nos. 1–3, pp. 670–672, 1989.
[6] D. Hauden, G. Jaillet, and R. Coquerel, "Temperature sensor using SAW delay line," in *Proc. IEEE Ultrason. Symp.*, Chicago, IL, USA, Oct. 1981, pp. 148–151.
[7] H. Scherr, G. Scholl, F. Seifert, and R. Weigel, "Quartz pressure sensor based on SAW reflective delay line," in *Proc. IEEE Ultrason. Symp.*, San Antonio, TX, USA, 1996, vol. 1, no. 2, pp. 347–350.
[8] M. Jungwirth, H. Scherr, and R. Weigel, "Micromechanical precision pressure sensor incorporating SAW delay lines," *Acta Mechanica*, vol. 158, nos. 3–4, pp. 227–252, 2002.
[9] D. Webb, D. Forester, A. Ganguly, and C. Vittoria, "Applications of amorphous magnetic-layers in surface-acoustic-wave devices," *IEEE Trans. Magn.*, vol. MAG-15, no. 6, pp. 1410–1415, Nov. 1979.
[10] P. Smole *et al.*, "Magnetically tunable SAW-resonator," in *Proc. IEEE Int. Freq. Control Symp.*, no. 2, May 2003, pp. 903–906.
[11] M. Kadota, S. Ito, Y. Ito, T. Hada, and K. Okaguchi, "Magnetic sensor based on surface acoustic wave resonators," *Jpn. J. Appl. Phys.*, vol. 50, no. 7S, 2011, Art. no. 07HD07.
[12] W. Li, P. Dhagat, and A. Jander, "Surface acoustic wave magnetic sensor using galfenol thin film," *IEEE Trans. Magn.*, vol. 48, no. 11, pp. 4100–4102, Nov. 2012.
[13] P. Bocchiaro and A. Zamperini, "Surface acoustic wave based magnetic sensors," *Model. Meas. Methods Acoustic Waves Acoustic Microdevices*, pp. 355–380, Aug. 2013. doi: 10.5772/55220.
[14] W. Wang, Y. Jia, X. Liu, and S. He, "Development of a novel SAW current sensor based on the magnetostrictive effect," in *Proc. IEEE Int. Ultrason. Symp.*, Taipei, Taiwan, Oct. 2015, pp. 1–3.
[15] W. Wang, Y. Jia, X. Liu, Y. Liang, X. Xue, and Z. Du, "Enhanced sensitivity of temperature-compensated SAW-based current sensor using the magnetostrictive effect," *Smart Mater. Struct.*, vol. 26, no. 2, 2016, Art. no. 025008.
[16] H. Mishra *et al.*, "Control of the magnetic response in magnetic field SAW sensors," in *Proc. IEEE SENSORS*, Glasgow, U.K., Oct./Nov. 2017, pp. 1–3.
[17] J. Tong *et al.*, "Development of a magnetostrictive FeNi coated surface acoustic wave current sensor," *Appl. Sci.*, vol. 7, no. 8, p. 755, 2017.
[18] V. Polewczyk *et al.*, "Unipolar and bipolar high-magnetic-field sensors based on surface acoustic wave resonators," *Phys. Rev. Appl.*, vol. 8, no. 2, pp. 1–11, 2017.
[19] A. Kittmann *et al.*, "Wide band low noise love wave magnetic field sensor system," *Sci. Rep.*, vol. 8, no. 1, 2018, Art. no. 278.
[20] X. Liu *et al.*, "Self-biased vector magnetic sensor based on a Love-type surface acoustic wave resonator," *Appl. Phys. Lett.*, vol. 113, no. 8, 2018, Art. no. 082402.
[21] W. Wang, Y. Jia, X. Xue, Y. Liang, and Z. Du, "Grating-patterned FeCo coated surface acoustic wave device for sensing magnetic field," *AIP Adv.*, vol. 8, no. 1, 2018, Art. no. 015134.
[22] C. Caliendo, E. Verona, A. D'Amico, A. Furlani, G. Iucci, and M. V. Russo, "Surface acoustic wave humidity sensor," *Sens. Actuators B, Chem.*, vol. 16, nos. 1–3, pp. 288–292, 1993.
[23] J. Filipiak, L. Solarz, and G. Steczko, "Surface acoustic wave (SAW) vibration sensors," *Sensors*, vol. 11, no. 12, pp. 11809–11832, 2011.
[24] J. Devkota, P. R. Ohodnicki, and D. W. Greve, "SAW sensors for chemical vapors and gases," *Sensors*, vol. 17, no. 4, p. 801, 2017.
[25] K. Länge, B. E. Rapp, and M. Rapp, "Surface acoustic wave biosensors: A review," *Anal. Bioanal. Chem.*, vol. 391, no. 5, pp. 1509–1519, 2008.
[26] E. R. Hirst, W. L. Xu, J. E. Bronlund, and Y. J. Yuan, "Surface acoustic wave delay line for biosensor application," in *Proc. 15th Int. Conf. Mechatron. Mach. Vis. Pract.*, Auckland, New Zealand, Dec. 2008, pp. 40–44.
[27] G. Fischerauer, A. Mauder, and R. Müller, *Acoustic Wave Devices*. Hoboken, NJ, USA: Wiley, 2008, pp. 135–180.
[28] D. B. Sullivan, D. W. Allan, D. A. Howe, and F. L. Walls, "Characterization of clocks and oscillators," U.S. Dept. Commerce, Nat. Inst. Standards Technol., Boulder, CO, USA, NIST Tech. Note 1337, 1990.
[29] B. Schiek, I. Rolfes, and H.-J. Siweris, *Noise in High-Frequency Circuits and Oscillators*. Hoboken, NJ, USA: Wiley, 2006.
[30] M. F. Lewis, "Surface acoustic wave devices and applications: 6. Oscillators—The next successful surface acoustic wave device?" *Ultrasonics*, vol. 12, no. 3, pp. 115–123, May 1974.
[31] T. E. Parker, "Precision surface acoustic wave (SAW) oscillators," in *Proc. IEEE Ultrason. Symp.*, San Diego, CA, USA, Oct. 1982, pp. 268–274.
[32] T. E. Parker and G. K. Montress, "Precision surface-acoustic-wave (SAW) oscillators," *IEEE Trans. Ultrason., Ferroelectr., Freq. Control*, vol. UFFC-35, no. 3, pp. 342–364, May 1988.
[33] P. Durdaut, M. Höft, J.-M. Friedt, and E. Rubiola, "Equivalence of open-loop and closed-loop operation of SAW resonators and delay lines," *Sensors*, vol. 19, no. 1, p. 185, 2019.

[34] P. Durdaut, A. Kittmann, A. Bahr, E. Quandt, R. Knöchel, and M. Höft, "Oscillator phase noise suppression in surface acoustic wave sensor systems," *IEEE Sensors J.*, vol. 18, no. 12, pp. 4975–4980, Jun. 2018.
[35] R. Ziemer, *Principles of Communication: Systems, Modulation and Noise*, 6th ed. Hoboken, NJ, USA: Wiley, 2009.
[36] *IEEE Standard Definitions of Physical Quantities for Fundamental Frequency and Time Metrology—Random Instabilities*, IEEE Standards 1139-2008, Feb. 2009.
[37] E. Rubiola, *Phase Noise and Frequency Stability in Oscillators*. Cambridge, U.K.: Cambridge Univ. Press, 2009.
[38] R. Boudot and E. Rubiola, "Phase noise in RF and microwave amplifiers," *IEEE Trans. Ultrason., Ferroelectr., Freq. Control*, vol. 59, no. 12, pp. 2613–2624, Dec. 2012.
[39] J. Rutman, "Characterization of phase and frequency instabilities in precision frequency sources: Fifteen years of progress," *Proc. IEEE*, vol. 66, no. 9, pp. 1048–1075, Sep. 1978.
[40] R. J. M. van de Veerdonk *et al.*, "1/f noise in anisotropic and giant magnetoresistive elements," *J. Appl. Phys.*, vol. 82, no. 12, pp. 6152–6164, Dec. 1997.
[41] E. Rubiola and V. Giordano, "Advanced interferometric phase and amplitude noise measurements," *Rev. Sci. Instrum.*, vol. 73, no. 6, pp. 2445–2457, Jun. 2002.
[42] J. A. Barnes *et al.*, "Characterization of frequency stability," *IEEE Trans. Instrum. Meas.*, vol. IM-20, no. 2, pp. 105–120, May 1971.
[43] S. R. Stein, "The allan variance–challenges and opportunities," *IEEE Trans. Ultrason., Ferroelectr., Freq. Control*, vol. 57, no. 3, pp. 540–547, Mar. 2010.

Phillip Durdaut (S'17) received the B.Eng. degree in information and electrical engineering from the University of Applied Sciences Hamburg, Hamburg, Germany, in 2013, and the M.Sc. degree in electrical engineering and information technology from Kiel University, Kiel, Germany, in 2015. He is currently pursuing the Dr.Ing. degree with the Chair of Microwave Engineering, Kiel University.

His main research interests include electronics with maximum signal-to-noise ratio for sensor systems based on thin-film magnetoelectric- and SAW sensors.

Anne Kittmann received the B.Sc. and M.Sc. degrees in material science and engineering from Kiel University, Kiel, Germany, in 2012 and 2015, respectively. She is currently pursuing the Dr.Ing. degree with the Chair of Inorganic Functional Materials, Kiel University, working on the development of sensors for magnetic field measurement.

Her research focus is on thin-film magnetoelectric- and surface acoustic wave sensors with high sensitivity and lowest limit of detection.

Enrico Rubiola (M'04) received the M.S. degree in electronics engineering from the Politecnico di Torino, Turin, Italy, in 1983, the Ph.D. degree in metrology from the Italian Ministry of Scientific Research, Rome, Italy, in 1989, and the D.Sc. degree in time and frequency metrology from the University of Franche-Comté (UFC), Besançon, France, in 1999.

He has been a Researcher with the Politecnico di Torino, a Professor with the University of Parma, Parma, Italy, and Université Henri Poincaré, Nancy, France, and a Guest Scientist with the NASA Jet Propulsion Laboratory, Pasadena, CA, USA. He has been a Professor with UFC and a Scientist with the Centre National de la Recherche Scientifique, Franche Comté Électronique Mécanique Thermique et Optique-Sciences et Technologies Institute, Besançon, since 2005, where he currently serves as the Deputy Director of the Time and Frequency Department. He has also investigated various topics of electronics and metrology, namely, navigation systems, time and frequency comparisons, atomic frequency standards, and gravity. His current research interests include precision electronics, phase-noise, amplitude-noise, frequency stability and synthesis, and low-noise oscillators from the low RF region to optics. He is the PI of the Oscillator IMP Project, a platform for the measurement of short-term frequency stability and spectral purity.

Jean-Michel Friedt received the Ph.D. degree in 2000.

He was a Post-Doctoral Fellow with IMEC, Leuven, Belgium, involved in acoustic and optical biosensors for characterizing organic thin-film properties before joining the Group of S. Ballandras in 2004 at FEMTO-ST, Besançon, France, for the development of passive sensors interrogated through a wireless link. He has been an Engineer with the company SENSeOR since its creation in 2006, hosted by the Time and Frequency Department of FEMTO-ST. His research interests include scanning probe microscopy, passive radio-frequency sensors and the associated radar-like electronics implemented as software-defined radio, and the combination of optical and acoustic methods for characterizing thin films.

Eckhard Quandt received the Diploma and Dr.Ing. degrees in physics from the Technische Universität Berlin, Germany, in 1986 and 1990, respectively.

He is currently a Professor with Kiel University, Kiel, Germany, where he is the Director of the Institute for Materials Science. He is the spokesperson for the DFG CRC 1261 Magnetoelectric Sensors: From Composite Materials to Biomagnetic Diagnostics. He is a member of Acatech, National Academy of Science and Engineering. His scientific focus is material research on smart materials and multiferroics and the development of sensors and actuators for microelectromechanical systems and nanoelectromechanical systems using such materials.

Reinhard Knöchel (M'88–SM'90–F'08–LF'18) received the Dipl.Ing. degree in electrical engineering and the Dr.Ing. degree from the Technical University, Braunschweig, Germany, in 1975 and 1980, respectively.

From 1980 to 1986, he was a Principal Scientist with the Philips Research Laboratory, Hamburg, Germany. In 1986, he joined the Hamburg University of Technology, where he was a Full Professor of Microwave Electronics until 1993. From 1993 to 2013, he held the Chair in Microwave Engineering, Kiel University, Kiel, Germany. His research interests include magnetic field sensors, active and passive microwave components, ultrawideband technology, microwave measurement techniques, and industrial microwave sensors and radar.

Michael Höft (M'04–SM'08) received the Dipl.Ing. degree in electrical engineering and the Dr.Ing. degree from the Hamburg University of Technology, Hamburg, Germany, in 1997 and 2002, respectively.

From 2002 to 2013, he was with the Communications Laboratory, European Technology Center, Panasonic Industrial Devices Europe GmbH, Lüneburg, Germany. He was a Research Engineer and a Team Leader, where he was involved in the research and development of microwave circuitry and components, particularly filters for cellular radio communications. From 2010 to 2013, he was also a Group Leader for the research and development of sensor and network devices. Since 2013, he has been a Full Professor with the Faculty of Engineering, Kiel University, Kiel, Germany, where he is the Head of the Chair of Microwave Engineering, Institute of Electrical Engineering and Information Technology. His research interests include active and passive microwave components, (sub-) millimeter-wave quasi-optical techniques and circuitry, microwave and field measurement techniques, microwave filters, microwave sensors, and magnetic field sensors. He is a member of the European Microwave Association, the Association of German Engineers, and the German Institute of Electrical Engineers.